Research Article | Vol. 11, No. 2 / 1 February 2020 / Biomedical Optics Express 660
Biomedical Optics EXPRESS

Improved optical slicing by stimulated emission depletion light sheet microscopy

JOSÉ MARTÍNEZ HERNÁNDEZ,[1] ALAIN BUISSON,[1] IRÈNE WANG,[2] AND JEAN-CLAUDE VIAL[2,*]

[1] *Univ. Grenoble Alpes, Inserm, U1216, Grenoble Institut Neurosciences, 38000 Grenoble, France*
[2] *Univ. Grenoble Alpes, CNRS, Laboratoire Interdisciplinaire de Physique, 38000 Grenoble, France*
[*] *jean-claude.vial@univ-grenoble-alpes.fr*

Abstract: Three-dimensional microscopy is mandatory for biological investigation. We describe a stimulated emission depletion selective plane illumination microscope (STED-SPIM) that provides both ease of implementation and an efficient optical slicing. This self-aligned system is based on a single diode-pumped solid-state laser and phase masks made of simple cover glass. A three-fold reduction of the light sheet thickness is achieved together with an enhancement of the sheet uniformity. This method is validated by using fluorescent microspheres and thick slices of fixed and clarified mouse brain to provide an enhanced imaging of Alzheimer's disease models.

1. Introduction

Generally, three-dimensional (3D) imaging is mandatory for investigating the structure of biological specimens. 3D information can be reconstructed through slice-by-slice images of the structure of a specimen, in a way similar to mechanical slicing in histopathology [1] where a specimen becomes separated physically into thin slices. Mechanical slicing is still used in current medical analysis and able to provide high-quality images. However, this process is extremely time-consuming (up to one week) and destructive, so that it cannot be applied to the study of living specimen.

Several microscopy methods allow to independently image single slices within the sample, a property named *optical slicing*. For example, in confocal microscopy, the excitation light is focused into a tight spot and a pinhole is inserted in the detection path, in order to eliminate fluorescence emitted above and below the focal point and achieve optical slicing. However, the observation of 3D tissues is limited by light scattering in the excitation and detection paths. As a result, imaging depth in tissues is generally limited to 100 µm.

Light Sheet Microscopy (also called SPIM [2] for Single/Selective Plane illumination Microscopy), is a promising alternative for rapid 3D imaging and is widely used for studying biological tissues and living embryos. In this technique, the excitation laser, perpendicular to the direction of observation, illuminates only a thin slice (µm range) of the sample, which fluorescence emission is then imaged onto a camera. Since the SPIM technique is 'full field', it provides a good optical slicing with high speed. One important limitation of this method is that, using standard Gaussian beams, it is not possible to reduce the sheet thickness (to improve the axial resolution) while maintaining a large field of view. This is simply because a focused Gaussian beam (with a wavelength λ), with a narrow beam waist (w_0), would also possess a short Rayleigh length (z_R) that follows the law: $z_R = \pi w_0^2/\lambda$. This limitation can be overcome if non-Gaussian beams such as Bessel [3,4] or Airy beams [5] are employed since they have the desirably property of being non-diffracting. Unfortunately these beams include a significant amount of excitation light outside the central thin lobe. Combining such beams with two-photon excitation reduces this undesirable contribution [4], since fluorescence signal would vary as a quadratic function of the incident intensity, but it requires powerful and expensive picosecond or

#379646 https://doi.org/10.1364/BOE.379646
Journal © 2020 Received 7 Oct 2019; revised 17 Dec 2019; accepted 18 Dec 2019; published 8 Jan 2020

Biomedical Optics EXPRESS

femtosecond lasers. The Lattice light sheet microscopy [6] is another alternative but it is much more complicated to implement than a standard light sheet microscope.

This article presents our contribution that aims at enhancing light sheet microscopy by an approach based on stimulated emission depletion (STED). Several previous works have suggested to apply the principle of STED to SPIM [7,8,9,10,11], giving rise to the STED-SPIM method. Recently we provided a proof of concept of an original STED-SPIM setup based on a dual-wavelength laser and a self-aligned design [12]. We registered an enhancement of the axial resolution while maintaining a large field of view, as shown in Fig. 1. In this experiment, the width of the region emitting fluorescence is measured as a function of the axial position, either with an excitation beam alone or with both the excitation beam and a donut-shaped STED beam. Clearly, upon addition of the STED beam, the width of the emitted fluorescence trace becomes super-resolved i.e. it is reduced by depletion on the periphery. But interestingly, the divergence is not accentuated and is much lower than what can be expected for a Gaussian beam having a waist equal to the super-resolved beam waist (red-dotted simulated curve in Fig. 1(c)).

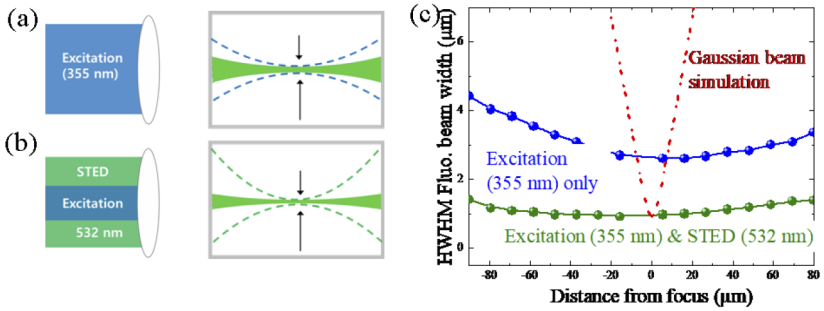

Fig. 1. (a and b respectively) Images of the fluorescence trace shown schematically with excitation (355 nm) alone and with donut-shaped STED beam (532 nm) added. (c) Experimental measurements of the beam width as a function of axial position, for the excitation beam alone (blue) and with the addition of a STED beam (from Ref. [12]). The red dotted curve is a simulation for a Gaussian beam having a beam waist identical to the experimental beam with STED (green curve)

Here, we demonstrate the same property, an enhanced axial resolution and field of view, by introducing two main improvements: a new design for the phase mask and an all-visible dual wavelength source. The conventional phase mask [13], which produces a donut shape for the stimulating beam leaving unaffected the pump beam, has a low efficiency and is ill suited to the light sheet necessities. Since a circular geometry of the stimulating beam is not necessary for STED-SPIM, we propose an important simplification of the phase mask which gains in efficiency. The original arrangement in an UV-Visible laser tandem was based on a harmonic generation from a pulsed Nd^{3+}:YAG laser, which provides self-aligned and synchronized pump at 355 nm and stimulating beams at 532 nm simultaneously. However UV excitation is often detrimental to the study of living biological samples. Here we have extended the concept to produce an all-visible tandem with self-aligned beams. The STED beam, in the yellow-red range, is produced by a 532 nm-pumped dye laser, while the exciting beam is the 532 nm beam itself. This tandem has nearly the same temporal characteristics as the previous one, but it reduces fluorophore bleaching [14] and induce less endofluorescence. The efficiency of our STED-SPIM design is demonstrated by the 3D characterization of fluorescent microspheres embedded in a gel and finally tested on real biological samples.

Biomedical Optics EXPRESS

2. Material and methods

The various elements for the STED-SPIM experiment are shown in Fig. 2. In order to perform STED in Coumarin 490 and CY3, we used two different laser tandems, Tandem-1 and Tandem-2, respectively. Both have self-aligned and self-synchronized excitation and stimulation beams. In Tandem-1, a nanosecond self Q-switched Nd:YAG laser (1064 nm, 10 to 130 kHz repetition rate, SNP models from TEEM-Photonics Inc., France) produces a 532 nm beam by second harmonic generation (SHG) in a potassium titanyl phosphate (KTP) crystal. Additionally a 355 nm beam is generated by sum frequency generation (SFG) of the residual 1064 nm and 532 nm in a beta barium borate (BBO) crystal. In Tandem-2, a more powerful 0.5-nanosecond self Q-switched Nd:YAG laser (1064 nm, 1 kHz repetition rate, PNP model from TEEM-Photonics) is frequency-doubled to generate a 532 nm beam. This 532 nm beam is used not only for excitation but also for generating a red beam (with wavelength from 600 to 630 nm) by pumping a Rhodamine 101 or Pyrromethene 650 dye laser. The dye laser cavity is obtained by the two parallel semi-reflective faces of a 1-cm dye cuvette (model 119.000F-QS from Hellma Inc.) perfectly perpendicular to the pump beam. Therefore the partially transmitted 532 beam and the red beam are collinear. The efficiency of this simple dye laser is 25% with the Rhodamine dye. For the two tandems, additional lenses (not shown on the figure) are used to ensure a milli-radian divergence and a ~mm diameter for the beams immediately after the tandem. For Tandem-1, the two beams are perfectly overlapped temporally. On the other hand, for Tandem-2, the two pulses partially overlap: the red pulse, of 400 ps duration, has a maximum delayed by ~ 100 ps from the maximum of the 532 nm pulse. This delay may cause a small fraction of the excited dye population to decay before it can be quenched by the stimulation pulse. However, the fluorescence lifetime of the dyes used in our experiment (~ 4 ns) being much longer than the delay, this effect can be neglected. On the contrary, a short delay can be beneficial since it prevents excited state absorption and the rate equations governing the depletion dynamics indicate a better STED efficiency when it is present [15]. Tandem 1 does not introduce a delay, the rate equations are now similar to CW-STED [16] and the STED efficiency is reduced but as analyzed in Ref. [12] the consequences are acceptable.

Our light sheet microscope (Fig. 2(d)) is a conventional scanned beam setup [17], with the addition of the dual-wavelength laser beam and a phase mask. The scanning mirror generates a light sheet parallel to the *xy* plane. The spherical lenses between the oscillating mirror and the light-sheet objective form a telescope to adapt the size of the beams and minimize their lateral displacement at the entrance of the objective. Depending on the objective used, the telescope magnification is modified (In some cases, the telescope is not present). The sample is attached to a piezoelectric translator, moving in the z direction, it allows the fast acquisition of stacks of images.

We have designed and characterized two types of dichroic phase masks that are able to produce an intensity null central stripe across the beam (as shown in Fig. 3(c)) at the stimulating wavelength λ_{STED}, while being perfectly transparent at the exciting wavelength λ_{ex}. Fundamentally they are both based on the diffraction from the phase edge of a transparent plate in transmission [18,19]. These two types are described in the following:

- Type 1 (Fig. 3(a)) mask is obtained by the assembly of two identical dual wavelength quartz waveplates (with a retardation of a half wave at λ_{STED} and a wave at λ_{ex}), their axis being crossed and the incident beam well centered at the interface between the two plates.

- Type 2 (Fig. 3(b)) mask is obtained using a single thin optical window (a microscope cover slip), which straight edge cuts through the middle of the incident beam, and which thickness e and refractive index $n(\lambda)$ are chosen to follow the law : $n(\lambda_{ex})e = p\lambda_{ex}$, $\quad n(\lambda_{STED})e = \frac{2p'+1}{2}\lambda_{STED}$ where p and p' are integers. It has been possible to find the correct thickness

Biomedical Optics EXPRESS

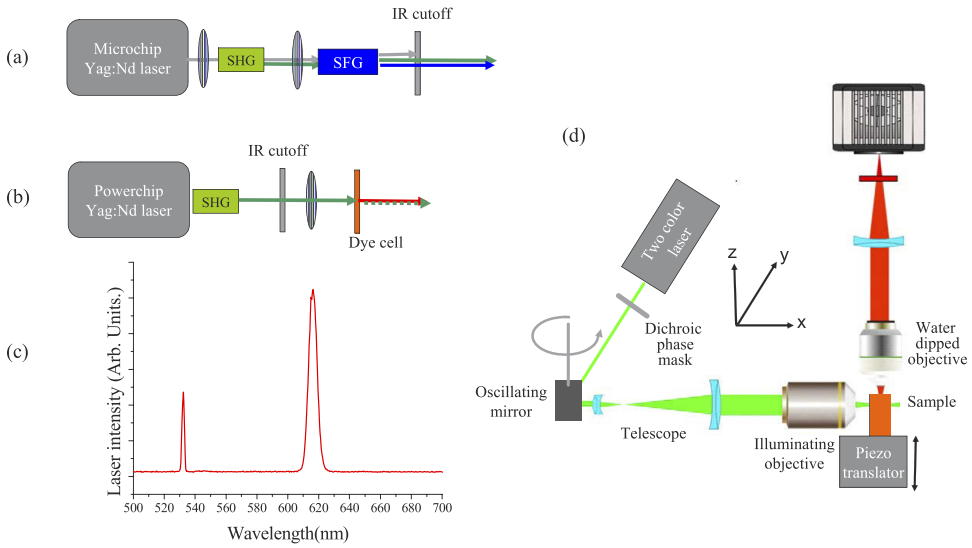

Fig. 2. (a) The UV-Vis laser tandem based on harrmonic generation (b) The all-visible laser tandem pumped by a 532 nm laser. The cavity is defined by the surface of the dye cell. The red output beam is collinear and synchronized with the 532 nm pulses. (c) The typical spectrum of the output of the all visible laser tandem when the dye used is the Pyrromethene 650. (d) Scheme of the experimental setup for STED-SPIM. The sheet produced by the oscillating mirror is in the horizontal xy plane and the sample is translated in the z direction.

within a set of a large number of cover slips since commercial cover slips have a small dispersion in thickness (170 ± 5 μm).

Figure 3(c) shows the light intensity distribution obtained for a well collimated Gaussian beam after passing through these masks. As expected, a dark sheet is created at λ_{STED} for both Type 1 and Type 2 phase masks. The two above solutions are perfect for monochromatic excitation but, when using the visible laser tandem (532 nm and red dye laser), the linewidth of the dye laser is far too broadband to be considered as monochromatic (7 nm, see Fig. 2(c)). In this case, a phase mask made of a single coverslip (even with the thinnest commercially available ones) cannot introduce a contrasted interference. The solution is found by juxtaposing two cover slips with a small difference in thickness, chosen among a large number of cover slips. The mounting of cover slips is certainly not perfect: in particular, the edge roughness of the cover slips are not documented by the vendor. Since the phase delay is not well-defined at the boundary, light incident in this region will partially fill up the zero intensity line. We tried to minimize this effect by using an illumination as large as possible, so that the fraction of stray light is small. We can suppose that the unwanted attenuation of the fluorescence at the center after stimulation (shown in Fig. 5(d)) is caused by this problem. For the future, a polishing of the edges can be envisaged.

STED-SPIM characterization is done by imaging fluorescence emission in simple dye solutions which absorption and emission spectra are well-matched with the excitation and depletion laser beams. Coumarin 490 is a common laser dye for blue operation [20], which is perfectly adapted for the 532-355 nm laser tandem. For the 532 nm-yellow to red tandem, the choice is very large: we have used the Rhodamine or Cyanine dyes (From Exciton). Fluorescent microspheres have been imaged to assess the resolution. They are impregnated with the same dyes (ref. FP60545-2 from Spherotec Inc.).

For the biological preparation of thick blocks of mouse brain (from a 12 months old mouse model of Alzheimer Disease) a clarification is necessary. We used a passive clarity protocol

Biomedical Optics EXPRESS

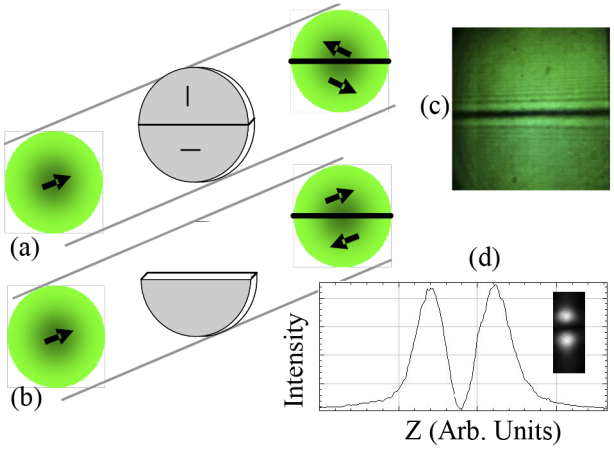

Fig. 3. (a) and (b) Type 1 and Type 2 phase masks, respectively, adapted for STED-SPIM and dichroic at 532-355 nm. The arrows represent the polarisation direction of the beam. (c) The image of the transmitted 532 nm non-scanned beam is taken in the near field. (d) The image of the same 532 nm beam but in the far field ie at the focus of a lens, the curve is its light intensity profile in the Z direction. The images are obtained with the Type 2 mask but the same result is obtained with the Type 1 mask. We have verified on a set of images taken at 355 nm (not shown here) that the beam is unaffected by these masks. The transmitted beams travelling along the y direction are scanned along the x direction to form the light sheet.

[21,22] since it gives better results for immunostaining. The fixed samples were incubated in hydrogel solution at 4°C under agitation for a week. To induce polymerization, we increase the temperature to 50°C in absence of oxygen. Once polymerized, we let the samples under agitation at 35-40°C in the clearing solution. This solution was renewed daily until the sample became completely transparent (for approximately 1 month). Then, the sample was washed in phosphate buffer (PBS) supplemented with 1% Triton and incubated in a solution of rabbit primary antibody raised against GFAP at 30 µg/mL (DAKO, France) for 48h at room temperature followed by several PBS washes. Next we performed a 48h incubation with the secondary antibody anti rabbit Cy3 at the concentration of 15 µg/ml (Jackson immunoresearch Lab, UK) followed by several washes to eliminate the excess. The embedding gel was chosen to have an index of refraction in between the index of water and that of the brain tissue. The gel should also preserve the integrity of the fragile brain tissue. We found that the best compromise is a pluronic gel [23] because it is prepared at low temperature, so that it does not damage the sample, and its refractive index can be adjusted by adding various fraction of glycerin and water to obtain a value as close as possible to the refractive index of the embedded objects.

All experiments on APP/PS1-1 mice were carried out in accordance with the European Community Council directives of November 24, 1986 (86/609/EEC) and with the French guidelines on the use of living animals in scientific investigations with the approval of the "Grenoble Institute of Neurosciences Ethical Committee".

3. Results and discussion

3.1. Experimental conditions

We have tried to adapt the experimental conditions to be compatible with the microscopy of biological samples. Concerning the laser powers, conventional Epifluorescence STED (E-STED) usually demands a high power for stimulation, in the range of 50 mW focused on a µm-sized

Biomedical Optics EXPRESS

spot i.e. an intensity in the order of MW/cm^2. In our case, as previously shown [12], the nanosecond pulse regime is particularly efficient and the excitation and the stimulation intensities are respectively reduced to 10 W/cm^2 and 10 kW/cm^2 for the UV-Vis tandem (with 140 kHz repetition rate). These powers are reduced when using the all visible laser tandem (1 kHz repetition rate) or when the beam is tightly focused by a high aperture lens (NA > 0.2). Under these conditions, the acquisition of a stack of 100 slices is performed in 5 seconds with the 140 kHz repetition rate laser, but it takes about a minute with the 1 kHz laser.

The depletion efficiency is first assessed by illuminating the samples with the bare stimulating beam i.e. without the phase mask. We then adapt the stimulating intensity as to obtain 90% to 95% extinction.

Photobleaching is not observed in solutions but is present on fluorescent nanospheres embedded in a pluronic gel, particularly when they are excited at 355 nm. We also observe photobleaching in the stained biological samples (excited at 532 nm). Nevertheless the lifetime of the dyes under our illumination conditions is long enough to allow the acquisition of about 20 successive stacks of 100 images at the same place.

3.2. The STED-SPIM components

A STED-SPIM microscope differs from an Epifluorescence STED (E-STED) microscope only in the direction of the illumination and stimulation beams. We used two collinear beams, one for excitation (the pump beam) and the other, spatially structured, for stimulation (the STED beam), that are scanned to form a sheet. As in E-STED, the stimulating beam is shaped by a phase mask in order to produce an intensity distribution overlapping the excitation beam but with zero intensity at the center. We have developed a convenient and efficient way to combine excitation and stimulating beams thanks to dual wavelength nanosecond lasers and dichroic phase masks. This setup is self-aligned, since excitation and stimulation beams are collinear by design, and requires few optical components.

3.3. Optimization of the phase masks

Dichroic phase mask have been used in E-STED microscopy to produce a donut-shaped focus spot [24]. In Ref. [12] we have shown that the conventional phase mask (to produce a donut-shaped stimulating beam) can also be used for STED-SPIM. However, when tightly focused, the beam did not display a total extinction at the donut center. This causes a noticeable fluorescence quenching at the center, which is undesirable. We have attributed this problem to the imperfections of the phase mask. It consisted of an assembly of four quadrant dual wavelength waveplates and it was difficult to have a perfect assembly. For STED-SPIM, the stimulating beam is now obtained in a different and simpler way by using a mask, which produces directly a zero intensity light sheet instead of a zero intensity central spot. The required phase mask is then simpler, since it can be made of only two halves in order to divide an incident beam into two sub beams with opposite phases. The behavior of this type of phase mask has been studied by Betz [18]. When placed in the laser beam path, it produces two sub beams separated by a dark stripe with remarkable divergences properties. In the near field, the central black stripe (shown on Fig. 3(c)) has a low divergence: its width varies as the square root of the distance from the mask. In the far field, the beam profile is well describe by a first order Hermite-Gauss [25,26] function with the usual linear divergence, which is identical to the Gaussian beam from which it originates. When a lens is placed after the mask, the behaviors in the far and near fields are reproduced at respective positions: close to the focus and out-of-focus. Figure 4 confirms this property: the divergence is similar to a Gaussian beam close to the focus, and becomes sub-Gaussian at longer distances. This observation suggests that, when possible, it can be interesting to use a slightly out of focus part of the STED beam for depletion. However, as seen Fig. 4(b) and Fig. 3(c), the two sub beams out of focus (corresponding to the near field of the phase plate), display additional faint

Biomedical Optics EXPRESS

side structures. This is expected since, in this range, the side ringing due to Fresnel diffraction by a sharp phase step is resolved while it is not resolved at focus, mainly because of the small aperture of the observing microscope lens. Nevertheless these side structures have negligible effect on the STED efficiency as shown in Fig. 5(c).

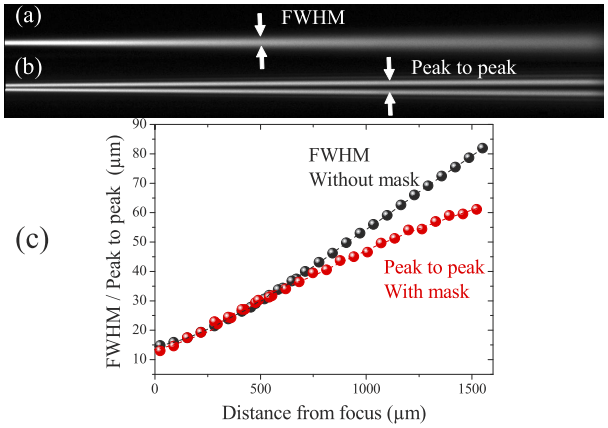

Fig. 4. Fluorescent traces in a Rhodamine dye solution excited by a 532 nm beam, focused by a 0.05 NA lens, without (a) and with (b) the two halves phase mask. (c) Measurement of the full width at half maximum of the beam, without mask, and the distance between the maxima of the two sub beams, when the mask is interposed, as a function of the distance of propagation from the focus.

3.4. STED fluorescence sheet characterization

When the double beam produced by the phase mask is used for STED, it is expected to narrow down the region that emits fluorescence. In addition, its interesting divergence properties can enhance the sheet thickness uniformity. In order to measure the thickness of the fluorescence sheets in the STED regime, we extracted the section of fluorescence traces imaged in a homogeneous solution using a microscope magnification and a CCD camera. Figure 5 shows the image of fluorescence sheets without and with STED under two focusing conditions. For both a moderate focusing and a tighter focusing, the thicknesses of the sheets are strongly reduced by STED. We can observe that there is no noticeable intensity loss for the moderate focusing, but a 50% intensity loss is observed for the finer sheet. We believe that this behavior can mainly be attributed to the still present imperfections of our phase masks. Spherical aberration of the focusing lens can also play a role. Indeed, in tight focusing conditions, the beam is affected by spherical aberration as it propagates through the dye cell, as shown in Fig. 1 and explained in Ref. [12]. Nevertheless 50% is not an inacceptable loss when balanced with the 4-fold increase in longitudinal resolution, particularly when also considering the improved uniformity over a large field of view. The 0.8 µm longitudinal resolution for example can compete advantageously with axial resolutions obtained with confocal or two photon microscopes.

Another way to characterize the STED-SPIM capability is to perform 3D imaging of well-defined microscopic objects. Commercially available fluorescent microspheres are perfectly adapted for this purpose. They are included in a pluronic gel [23] as a good index matching medium. A stack of images is acquired, the axial dimension (the z direction) being obtained by moving the sample. Figure 6 presents different views of a 25 µm z stack. The xy views (parallel to the light sheet) without and with stimulation are identical since, for theses directions, the resolution is only given by the observing lens and camera. But the orthogonal views shown in Fig. 6(b,c) depend on the sheet thickness. Without STED, the images of the microspheres are

Biomedical Optics EXPRESS

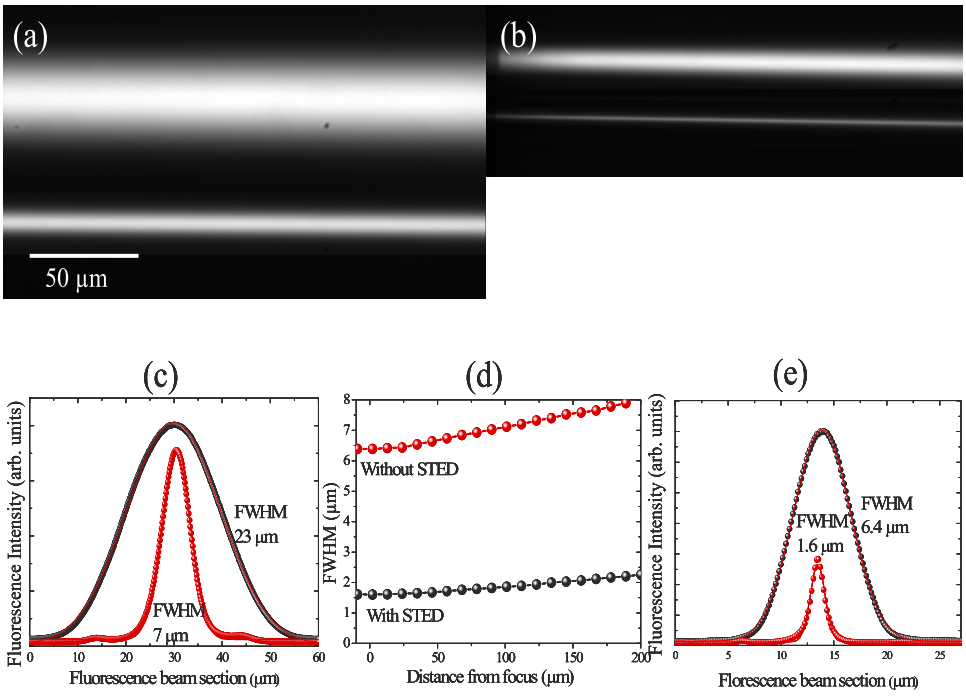

Fig. 5. Fluorescence light sheets in a Rhodamine dye cell excited at 532 nm and depleted at 600 nm : (a) low focusing, (b) high focusing with their respective beam waist section (c) and (e). The plot (d) is the fluorescence beam section as a function of the distance from focus measured on (b). Low focusing is obtained with a 150 mm focal length (NA around 0.025) while tighter focusing is obtained by a 40 mm focal length (NA around 0.1).

extended longitudinally (along the Z direction) since the light sheet is thicker than the microsphere diameters. On the other hand, their elongation is noticeably reduced with STED. A way to measure precisely the z resolution enhancement with STED is to select a microsphere image with and without STED and to plot its integrated fluorescence intensity as a function of the slice position in the stack (the z position). Figure 6(e) confirms a 300%resolution increase. Finally a decisive measurement of the resolution enhancement would be to perform the same kind of measurement for two microspheres in contact along the z direction but since the microsphere concentration is low it is impossible to find two microspheres having a high proximity and perfectly aligned along z simultaneously. In the zone delimited by a square in Fig. 6(a) the best situation is found: two microspheres with a high proximity along z and a shift as small as possible along x or y. In Fig. 7 the orthogonal views and a Z-linescan shows that an unresolved z-profile under the excitation alone becomes resolved by STED.

3.5. *Three dimensional imaging thick brain slices of transgenic animal model of Alzheimer's disease*

Understanding the molecular mechanisms underlying the pathological manifestations and progression of Alzheimer's disease (AD) [27] is crucial for developing effective as well as targeted therapies for those afflicted with this devastating disease. This work aims at presenting a convenient imaging method to help studying the amyloid-beta (Aβ) [28], the peptide that triggers AD pathology by mediating impairment of neuron/astrocyte interaction in the early phase of the disease. For this purpose we investigate astrocytes morphology by imaging at various resolutions, thick slices of APP/PS1 brain tissues, an animal model of Alzheimer's disease.

Biomedical Optics EXPRESS

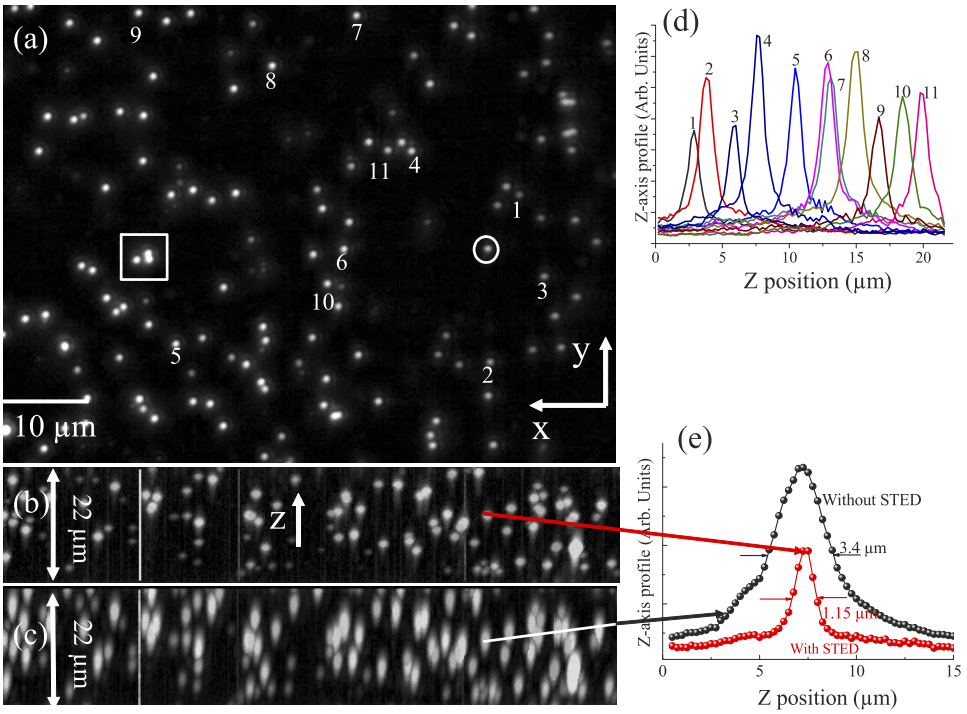

Fig. 6. (a). The Z projection (Average intensity) of a 25 µm thick stack of 100 images of fluorescent 0.4-0.6 µm diameter fluorescent microspheres embedded in a pluronic gel excited at 355 nm with stimulation depletion at 532 nm. (b). The X projection of the orthogonal views of the stack with STED. (c). The X projection of the orthogonal view for the same sample but without STED. (d). The Z axis profile of a set of microspheres measured on the stack under stimulation depletion, the microspheres are numbered from 1 to 11. (e) The Z-axis profile of a particular microsphere (surrounded in the image (a)) with and without depletion. The focusing lens has a 0.1 NA.

Imaging thick blocks of brain is less easy than imaging a fluorescent bead suspension because it is turbid and the roughness of the surfaces perturbs the wavefront of both excitation and detection. Two solutions are implemented: first, optical clarification to minimize light scattering and second, the inclusion of the sample in a gel to partially adapt the refraction index. This last procedure, together with the use of a water-immersion objective, minimizes wavefront distortion, at least on the imaging side.

We immunolabeled the glial fibrillary acidic protein (GFAP) a protein selectively expressed in astrocytes. GFAP, the main intermediate filament of astrocytes, is commonly used to visualize astrocyte morphology in the adult brain [29]. Combining clearing, labeling, embedding, and STED-SPIM with a water-immersion imaging objective allowed us to visualize the astrocytic network. Large bright plaques are also well resolved (Fig. 8(a,b)). They are attributed to the endofluorescence of pathological markers of AD, amyloid plaques, but a leaking of the Cy3 dye cannot be excluded. Medium magnification reveals a dense 3D network of astrocytes (Fig. 8(b)) and high magnification is able to resolve the 3D organization of their dense networks (Fig. 8(c)).

The resolution enhancement expected from STED is less easy to characterize than for the microspheres suspensions. For the biological samples, in all cases, it is necessary to acquire the images as close as possible to the illumination side (on the left of Fig. 8(a)). The quality of the images and the STED slicing efficiency rapidly decrease as we try to move further from the

Biomedical Optics EXPRESS

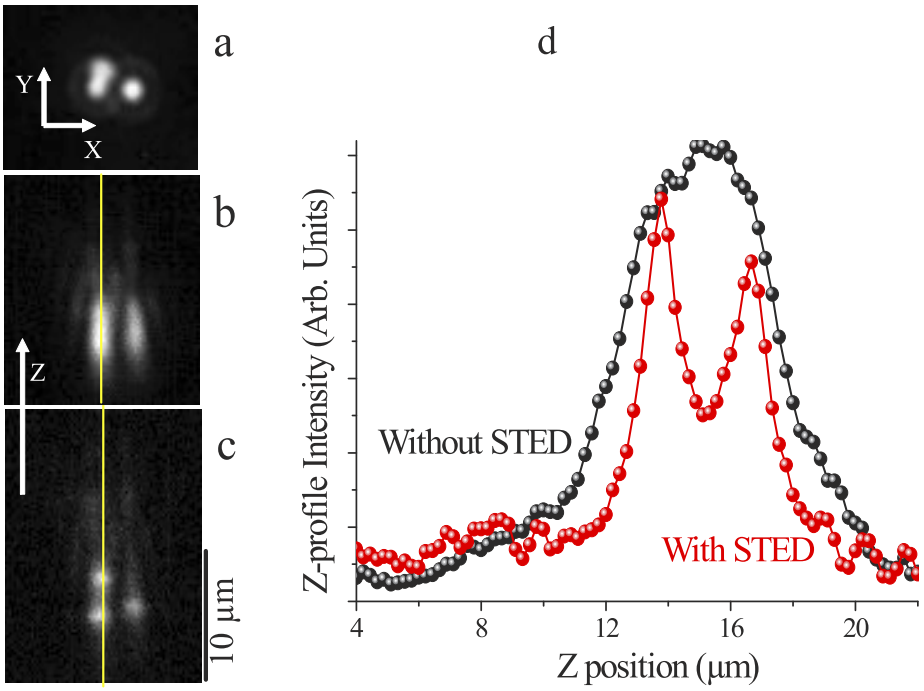

Fig. 7. The Z profile of two contacted microspheres along the Z direction. (a). A zoom of the zone delimited by a square in Fig. 6(a). (b) The orthogonal view of the stack without STED. (c) The orthogonal view of the stack with STED. (d) The Z-profile along the yellow lines in (b) and (c).

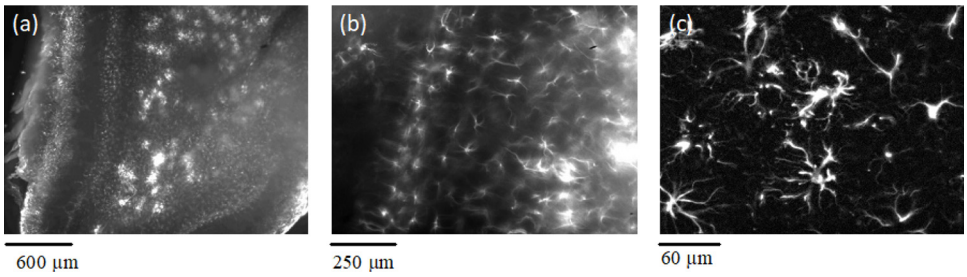

Fig. 8. Images at various magnification of a block of 12 months old cleared AD mouse (APP:PS1-21 lines) brain embedded in a pluronic gel, the astrocytes are anti-GFAP/CY3 stained (a) Z projection of a 100 µm thick stack (2.2mm×1.8mm). The bright zones are amyloid plaques. The imaging objective (×4) has a NA=0.15 giving a lateral resolution of about 2µm. The focal length of the focusing lens for illumination is 100 mm giving also a super-resolved sheet thickness of ~2µm. (b) An optical slice taken at 40 µm below the surface. The water-immersion objective (×10) for imaging has a NA=0.3 giving a lateral resolution of about 1µm. The focal length of the focusing lens for illumination is 50 mm giving a super-resolved sheet thickness around 1µm. (c) Z projection of 10 optical slices (0.1 µm thick) taken at 10 µm below the surface. The water-immersion objective (×40) for imaging has a NA=0.5 giving a lateral resolution around 0.5µm. The focal length of the focusing lens for illumination is 25 mm giving also a super-resolved sheet thickness around 0.5 µm.

Biomedical Optics EXPRESS

entrance interface. This can be attributed to the roughness of this interface, since it was difficult to perfectly cut the brain block and the index of refraction of the pluronic gel was not sufficiently adapted to compensate for the roughness. The consequence is double: first light scattering occurs and blurs the image, secondly a strong wavefront perturbation is certainly present and affects the strict relation between the phases introduced by the mask and, hence, the intensity contrast of the central stripe in the STED beam. In these experiments, the lens on the illumination side was a dry lens. We believe that a water-immersion objective lens, such as those used in intravital microscopy, should partially solve the problem of index mismatch at the interface.

4. Conclusion

This work present progress in 3D optical imaging by using STED-SPIM to achieve higher spatial resolution and improved optical slicing. By simply coupling a two-color laser equipped with a rudimentary phase mask into a SPIM microscope, we obtain a strong reduction of the fluorescent sheet thickness. An additional benefit is that the super-resolved sheets are more extended than the initial ones. 3D imaging of thick suspension of fluorescent microspheres in a gel allowed us to verify that the sheet thinning enhances axial resolution by a factor of 300%. Precisely, with moderate laser power, a Point Spread Function (PSF) extension in the Z direction of 1.1 µm over a field of view of 500 µm is attained.

Similar performances can be obtained with setups such as two-photon Bessel beam light sheet microscopy [4] or lattice light sheet microscopy where the structured illumination enhances the resolution. These methods are mature and adapted to living samples [30], it is difficult to compare them with this STED-SPIM method since it is only checked on fixed samples, but we believe that the interesting performances of the present design mainly originate from the efficient stimulation and low phototoxicity induced by the dual color nanosecond laser, due to its temporal characteristics. Note that the moderate repetition rate of these lasers becomes acceptable in SPIM modality. In addition as often pointed out [31] the STED phenomenon can give an unlimited resolution improvement as soon as the stimulation power can be tolerated by the sample, which is not the case for the other alternatives. This new STED-SPIM design allows imaging of thick clarified block of mouse brain at various scales. Nevertheless, before this technique can be used in routine way, more experiments are certainly needed to characterize the sensitivity of STED-SPIM to wavefront perturbations. Additionally a better staining minimizing the bleaching and a careful preparation of the sample, principally on the illumination side, are mandatory.

Funding

Agence Nationale de la Recherche.

Disclosures

The authors declare that there are no conflicts of interest related to this article.

References

1. M. Ragazzi, S. Piana, C. Longo, F. Castagnetti, M. Foroni, G. Ferrari, G. Gardini, and G. Pellacani, "Fluorescence confocal microscopy for pathologists," Mod. Pathol. **27**(3), 460–471 (2014).
2. P. A. Santi, "Light sheet fluorescence microscopy: a review," J. Histochem. Cytochem. **59**(2), 129–138 (2011).
3. J. Durnin, J. J. Miceli, and J. H. Eberly, "Diffraction-Free Beams," Phys. Rev. Lett. **58**(15), 1499–1501 (1987).
4. F. O. Fahrbach, V. Gurchenkov, K. Alessandri, P. Nassoy, and A. Rohrbach, "Light-sheet microscopy in thick media using scanned Bessel beams and two-photon fluorescence excitation," Opt. Express **21**(11), 13824–13839 (2013).
5. T. Vettenburg, H. I. Dalgarno, J. Nylk, C. Coll-Llado, D. E. Ferrier, T. Cizmar, F. J. Gunn-Moore, and K. Dholakia, "Light-sheet microscopy using an Airy beam," Nat. Methods **11**(5), 541–544 (2014).
6. B. C. Chen, W. R. Legant, K. Wang, L. Shao, D. E. Milkie, M. W. Davidson, C. Janetopoulos, X. F. S. Wu, J. A. Hammer, Z. Liu, B. P. English, Y. Mimori-Kiyosue, D. P. Romero, A. T. Ritter, J. Lippincott-Schwartz, L. Fritz-Laylin, R. D. Mullins, D. M. Mitchell, J. N. Bembenek, A. C. Reymann, R. Bohme, S. W. Grill, J. T. Wang, G. Seydoux,

Biomedical Optics EXPRESS

U. S. Tulu, D. P. Kiehart, and E. Betzig, "Lattice light-sheet microscopy: Imaging molecules to embryos at high spatiotemporal resolution," Science **346**(6208), 1257998 (2014).
7. M. Friedrich, Q. Gan, V. Ermolayev, and G. S. Harms, "STED-SPIM: Stimulated emission depletion improves sheet illumination microscopy resolution," Biophys. J. **100**(8), L43–L45 (2011).
8. P. Zhang, P. M. Goodwin, and J. H. Werner, "Fast, super resolution imaging via Bessel-beam stimulated emission depletion microscopy," Opt. Express **22**(10), 12398–12409 (2014).
9. C. Gohn-Kreuz and A. Rohrbach, "Light-sheet generation in inhomogeneous media using self-reconstructing beams and the STED-principle," Opt. Express **24**(6), 5855–5865 (2016).
10. P. Hoyer, G. de Medeiros, B. Balázs, N. Norlin, C. Besir, J. Hanne, H.-G. Kräusslich, J. Engelhardt, S. J. Sahl, S. W. Hell, and L. Hufnagel, "Breaking the diffraction limit of light-sheet fluorescence microscopy by RESOLFT," Proc. Natl. Acad. Sci. **113**(13), 3442–3446 (2016).
11. C. Gohn-Kreuz and A. Rohrbach, "Light needles in scattering media using self-reconstructing beams and the STED principle," Optica **4**(9), 1134–1142 (2017).
12. T. Scheul, I. Wang, and J. C. Vial, "STED-SPIM made simple," Opt. Express **22**(25), 30852–30864 (2014).
13. S. W. Hell and J. Wichmann, "Breaking the Diffraction Resolution Limit by Stimulated-Emission - Stimulated-Emission-Depletion Fluorescence Microscopy," Opt. Lett. **19**(11), 780–782 (1994).
14. G. Donnert, C. Eggeling, and S. W. Hell, "Triplet-relaxation microscopy with bunched pulsed excitation," Photochem. Photobiol. Sci. **8**(4), 481–485 (2009).
15. M. C. Chiang, J. C. Garcia, and J. M. Liu, "Depletion Dynamics for Stimulated Emission Depletion (STED) Microscopy," in *2008 Conference on Lasers and Electro-Optics & Quantum Electronics and Laser Science Conference*, Vols 1-9 (IEEE, 2008), pp. 250–251.
16. K. I. Willig, B. Harke, R. Medda, and S. W. Hell, "STED microscopy with continuous wave beams," Nat. Methods **4**(11), 915–918 (2007).
17. O. E. Olarte, J. Andilla, E. J. Gualda, and P. Loza-Alvarez, "Light-sheet microscopy: a tutorial," Adv. Opt. Photonics **10**(1), 111–179 (2018).
18. H. D. Betz, "An asymmetry method for high precision alignment with laser light," Appl. Opt. **8**(5), 1007–1013 (1969).
19. M. T. Tavassoly, S. R. Hosseini, A. M. Fard, and R. R. Naraghi, "Applications of Fresnel diffraction from the edge of a transparent plate in transmission," Appl. Opt. **51**(30), 7170–7175 (2012).
20. E. Schimitschek, J. Trias, P. Hammond, and R. Atkins, "Laser performance and stability of fluorinated coumarin dyes," Opt. Commun. **11**(4), 352–355 (1974).
21. K. Chung and K. Deisseroth, "CLARITY for mapping the nervous system," Nat. Methods **10**(6), 508–513 (2013).
22. I. Costantini, R. Cicchi, L. Silvestri, F. Vanzi, and F. S. Pavone, "In-vivo and ex-vivo optical clearing methods for biological tissues: review," Biomed. Opt. Express **10**(10), 5251–5267 (2019).
23. R. Blank and D. Mody. 1986. Patent "Stable hydrogen peroxide gels" American Home Products Corporation NY.
24. M. Reuss, J. Engelhardt, and S. W. Hell, "Birefringent device converts a standard scanning microscope into a STED microscope that also maps molecular orientation," Opt. Express **18**(2), 1049–1058 (2010).
25. S. Saghafi and C. J. R. Sheppard, "Near field and far field of elegantHermite-Gaussian and Laguerre-Gaussian modes," J. Mod. Opt. **45**(10), 1999–2009 (1998).
26. J. Enderlein and F. Pampaloni, "Unified operator approach for deriving Hermite-Gaussian and Laguerre-Gaussian laser modes," J. Opt. Soc. Am. A **21**(8), 1553–1558 (2004).
27. W. E. Klunk, C. J. Xu, R. J. McClure, K. Panchalingam, J. A. Stanley, and J. W. Pettegrew, "Aggregation of beta-amyloid peptide is promoted by membrane phospholipid metabolites elevated in Alzheimer's disease brain," J. Neurochem. **69**(1), 266–272 (2002).
28. L. Nagel-Steger, B. Demeler, W. Meyer-Zaika, K. Hochdorffer, T. Schrader, and D. Willbold, "Modulation of aggregate size- and shape-distributions of the amyloid-beta peptide by a designed beta-sheet breaker," Eur. Biophys. J. **39**(3), 415–422 (2010).
29. L. F. Eng, R. S. Ghirnikar, and Y. L. Lee, "Glial fibrillary acidic protein: GFAP-thirty-one years (1969-2000)," Neurochem. Res. **25**(9/10), 1439–1451 (2000).
30. T. A. Planchon, L. Gao, D. E. Milkie, M. W. Davidson, J. A. Galbraith, C. G. Galbraith, and E. Betzig, "Rapid three-dimensional isotropic imaging of living cells using Bessel beam plane illumination," Nat. Methods **8**(5), 417–423 (2011).
31. B. Harke, J. Keller, C. K. Ullal, V. Westphal, A. Schoenle, and S. W. Hell, "Resolution scaling in STED microscopy," Opt. Express **16**(6), 4154–4162 (2008).